CHAPTER IV
SYNTHESIS OF Fe-SBA-15, Mo-SBA-15, AND Ti-SBA-15 VIA SOL-GEL PROCESS OF SILATRANE AND ACTIVITY STUDY OF Ti-SBA-15

4.1 Abstract

The synthesis of M-SBA-15 (M = Fe, Mo, and Ti) was successfully achieved via a simple and energy-saving sol-gel process, called a novel room temperature synthesis route, using a moisture-stable silatrane as a silica precursor and a triblock copolymer PEO_{20}-PPO_{70}-PEO_{20} as a structure-directing agent. Ferric chloride, molybdenum glycolate, and titanium glycolate were used as metal sources. The reaction took place in an acidic media at room temperature. The SAXS patterns of all sample showed two well-defined peaks which are characteristic of SBA-15. N_2 adsorption/desorption isotherms clearly showed type IV isotherm with H1-type hysteresis loop which is the characteristic of mesoporous materials, having narrow pore size distribution and large pore diameter. TEM images confirmed the formation of the regular hexagonal mesopore array. DRUV results indicated that most of the metal ions were incorporated into the SBA-15 framework. The catalytic activity of the Ti-SBA-15 catalysts was investigated via oxidation reaction of styrene and it exhibited higher activity than pure SBA-15. The products form this reaction were only styrene oxide and benzaldehyde.

4.2 Introduction

So-called SBA-15 (2D well-ordered hexagonal mesoporous silica) is an excellent support for any catalysts because of its high surface area, large pore size, and thick wall [1]. Many metals, for examples, Fe, Ti and Mo, show a great catalytic performance in many reactions [2–4], especially, the oxidation reaction. Therefore, numerous researchers have paid much attention to develop methods to incorporate metal atoms into the framework of SBA-15.

In term of synthesis, Zhang and coworkers [5] prepared highly ordered Fe-SBA-15 by physical-vapor-infiltration. This method is quite complicated and results

in lower surface area and pore diameter of the products. Li and coworkers [6] proposed the direct hydrothermal method for synthesizing highly ordered Fe-SBA-15 in 2005. The obtained products had relatively high surface area, large pore size, and high amount of iron (10%) incorporated into the SBA-15 framework. In 2002, Zhang *et al.* [7] developed a new approch for synthesizing Ti-SBA-15 materials by accelerating the hydrolysis of silicon precursor (tetramethoxysilane, TMOS) using fluoride. The Ti-SBA-15 samples obtained from this route had high quality, however, the titanium contents in the silica framework were quite low ($\leq$ 1%). In 2007, Melero *et al.* [8] successful prepared highly dispersed Mo-SBA-15 using a co-condensation method. The prepared Mo-SBA-15 showed high mesoscopic ordering degrees, narrow pore size distribution, and high dispersion of metal oxide.

In our earlier report, the simple and energy-saving approch used to synthesize SBA-15 mesoporous silica via sol-gel process of silatrane was discovered [9]. The SBA-15 product could be obtained just by stirring at room temperature and had equal quality to those prepared from other thermal-assisted methods. Therefore, in this work, this novel method was extended to the preperation of highly ordered Fe-Mo-, and Ti-SBA-15 materials. The structural and physical properties of these samples were evaluated as well as the catalytic activity of Ti-SBA-15 was investigated.

4.3 Experimental

4.3.1 Materials

Fumed silica (SiO_2, 99.8%, Sigma-Aldrich, USA), triethanolamine (TEA, Carlo Erba), ethylene glycol (EG, J,T. Baker, USA), acetronitrile (Labscan, Asia), poly(ethylene glycol)-block-poly(propylene glycol)-block-poly(ethylene glycol) ($EO_{20}PO_{20}EO_{20}$) (P123, Sigma-Aldrich, USA), hydrochloric acid (HCl, Labscan, Asia), ferric chloride ($FeCl_3$, Sigma-Aldrich, USA), titanium oxide (TiO_2, Sigma-Aldrich, USA), triethylenetetramine (TETA, Facai polytech, Thailand), molybdenum oxide (MoO_3) (Fluka), and 30% hydrogenperoxide (30% H_2O_2, Carlo Erba) were directly used without further treatment.

4.3.2 Synthesis of Silatrane Precursor [10]

Siatrane precursor was synthesized via Oxide One Pot Synthesis (OOPS) process by mixing SiO_2 and TEA in a simple distillation set using EG as solvent. Reaction was heated to 200 °C under N_2 atmosphere and kept running for 10 hr. Then, EG was removed under vacuum to obtain crude solid product which was washed with acetonitrile and dried in desiccator.

4.3.3 Synthesis of Molybdenum Glycolate Precursor [11]

Molybdenum glycolate was synthesized by mixing MoO_3 (4.29g) and EG (50 mL) with vigorously stirring and heating to 150 °C under N_2 atmosphere for 15 min. The obtained solution was centrifuged to separate the unreacted MoO_3. The solution part was left at room temperature for 3 days to obtain molybdenum glycolate solid, followed by washing with acetronotrile and drying in desiccator.

4.3.4 Synthesis of Titanium Glycolate Precursor [12]

Titanium glycolate was synthesized by mixing TiO_2 (2 g) and TETA (3.65 g) with stirring vigorously in excess EG (25 mL), and heating to 200 °C for 24 hr. The resulting solution was centrifuged to separate the unreacted TiO_2. The excess EG and TETA was removed by vacuum distillation to obtain a crude precipitate. The white solid product was washed with acetonitrile, dried in a vacuum desiccator.

4.3.5 Synthesis of M-SBA-15 (M = Fe, Mo, and Ti) [9]

M-SBA-15 was synthesized using silatrane as a silica precursor and non-ionic triblock copolymer surfactant $EO_{20}PO_{70}EO_{20}$ as a template. Iron chloride ($FeCl_3$), molybdenum glycolate, and titanium glycolate were used as iron, molybdenum and titanium sources, respectively. HCl aqueous was used as an acid source.

The preparation procedure of M-SBA-15 materials was described as follows: 2 g of P123 was dissolved in 40 mL of 2M HCl (solution A) and 4.5 g of silatrane was mixed with 10 ml of deionized water to get solution B. Solution A and solution B were stirred at room temperature for 1 hr. Then, solution B and calculated amount of metal precusors were added to solution A and kept stirring at room temperature for 24 hr. After that, the resultant solid was filtered, washed with deionized water, dried at ambient temperature overnight, and, then, calcined at 550 °C for 6 hr.

4.3.6 Characterization of Precursors and M-SBA-15 Samples.

Thermal gravimetric analysis were carried out using TG-DTA (Pyris Dimond Perkin Elmer) with a heating rate of 10 °C/min in a range of room temperature to 750 °C under nitrogen atmosphere to determine the thermal stability of silatrane, molybdenum glycolate and titanium glycolate. Fourier-transform infrared (FT-IR) absorption spectrometer (Nicolet, NEXUS 670) at a resolution of 2 cm^{-1} were used to examine the functional groups of the precursors. Small-angle X-ray scattering (SAXS) patterns were obtained with a PANalytical PW3830 X-ray instrument using CuKα radiation generated at 50kV and 40 mA to investigate the crystallinity of the catalysts. TEM images were carried out to study the mesoporous order of synthesized M-SBA-15 materials on a JEOL JEM-2100F TEM instrument operated at an accelerating voltage of 200 kV with a large objective aperture. Nitrogen sorption isotherms were obtained at the temperature of liquid nitrogen after out gassing at 250°C for 20 hr (Quantasorb JR, Mount Holly, NJ). The surface area was determined by the Brunauer–Emmett–Teller (BET) method. Diffuse reflectance UV-vis spectra were obtained using SHIMADZU UV 2550-VISSIBLE spectrophotometer in the region of 200-600 nm to detect the framework and extra-framework of iron, molybdenum and titanium species.

4.3.7 Catalytic Activity Study of Ti-SBA-15.

The catalytic activity of the catalyst was studied using the selective oxidation reaction of styrene. Five mmol of styrene, 5 mmol of 30 % H_2O_2, (*x*) g of catalyst and 10 mL of acetonitrile were mixed in a 50 mL glass flask and heated to certain temperature. The products were analyzed using a GC equipped with FID detector. The studied factors were reaction temperature, reaction time, amount of catalyst used, and amount of Ti loaded. The conversion of styrene were calculated on the basis of the amount of styrene monomer used.

4.4 Results and Discussion

4.4.1 Characterization of Silatrane, Molybdenum Glycolate, and Titanium Glycolate Precursors

These precursors were synthesized by the Oxide One Pot Synthesis (OOPS) process. The obtained product of silatrane is a white powder whose structure is shown in Figure 4.1. Its TGA result (Figure 4.2a) shows one major transition of weight loss at 380 °C with 19.5 % ash yield, corresponding to $Si((OCH_2CH_3)_3N)_2H_2$ having 18 % theoretical ceramic yield. In addition, FTIR spectrum (Figure 4.2b) also shows characteristic peak of silatrane at 785–729 and 579 cm^{-1}, corresponding to Si-O-C and Si ◄·····N, respectively [10].

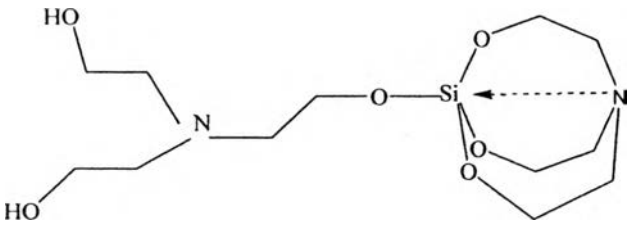

Figure 4.1 The structure of silatrane precursor.

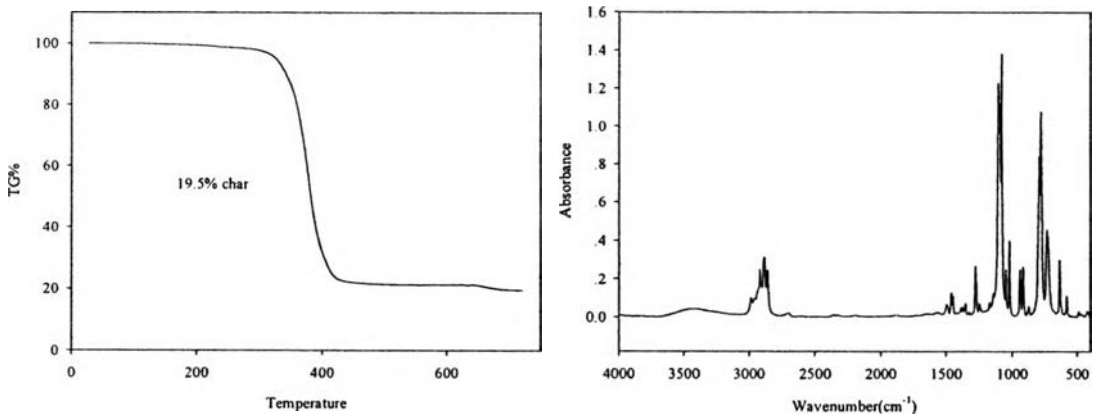

Figure 4.2 (a) TGA and (b) FTIR results of silatrane precursor.

The structure of molybdenum glycolate is shown in Figure 4.3. The product obtained is white powder. Both TGA and FTIR results are in agreement with those reported in reference 11. There are, in the TGA result (Figure 4.4a), five mass loss transitions at 150 °C (H_2O molecule adsorbed by molybdenum glycolate, also

confirm by FTIR), 210 °C (H_2O molecule generated from decomposition of molybdenum glycolate), 350 °C (glycolate ligand of molybdenum glycolate molecule), 430 °C (the other ligand of molybdenum glycolate molecule), and 720 °C (carbon residues) with 45.6 % ash yield, corresponding to $Mo((OCH_2CH_2O)_2(OH)_2)$ having 56.7 % theoretical yield. When taking off the first mass loss of water adsorbed by the product, the ash yield became 55.61 % closer to the theoretical yield. For FTIR result (Figure 4.4b), the bands observed at 946 and 533 cm^{-1} are assigned to the Mo-O-C and Mo-O streching, respectively [11].

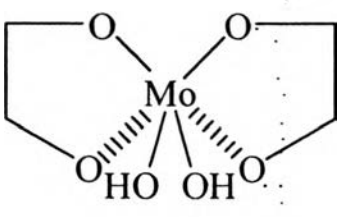

Figure 4.3 The structure of molybdenum precursor.

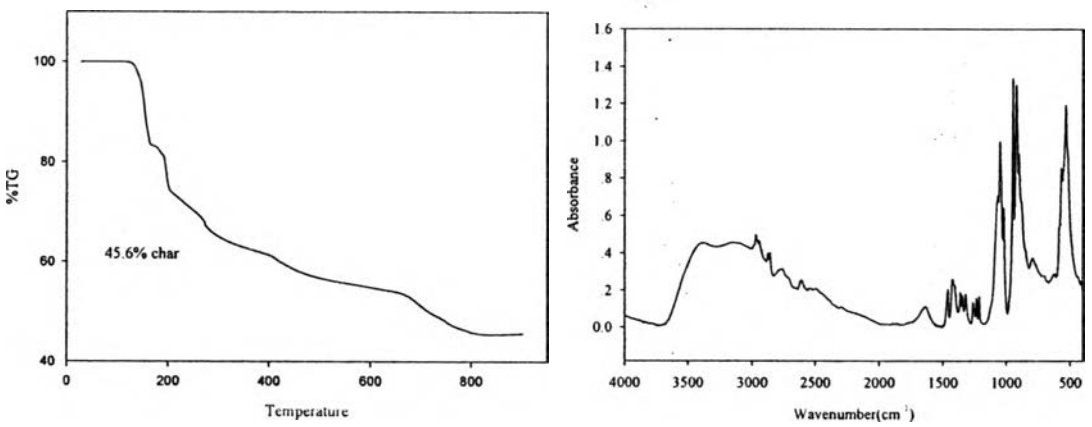

(a) **(b)**

Figure 4.4 (a) TGA and (b) FTIR results of molybdenum glycolate precursor.

Since, water is a by-product of the OOPS process, it must be removed from the system to push the reaction forward, as illustrated in the following equation.

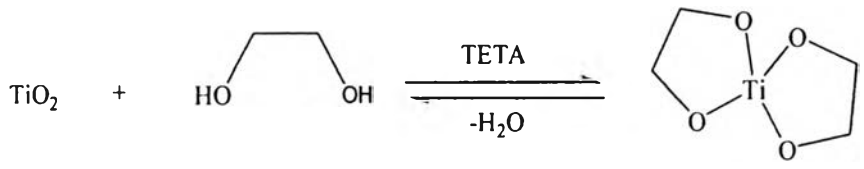

TGA thermogram of titanium glycolate was obtained in nitrogen atmosphere and the result is shown in Figure 4.5a. The weight loss around 310–350 °C corresponded to organic ligand decomposition. A small weight loss at around 100–250 °C referred to trace amounts of water and EG. The final ash yield was 52.0 % which is higher than the theoretical ceramic yield, 47.56 %, based on the product structure shown in the equation. FTIR spectrum (Figure 4.5b) showed the band around 2855–2927 cm^{-1} assigned to the C-H stretching of ethylene glycol ligand and the 1080 and 619 cm^{-1} bands, corresponding to C-O-Ti and Ti-O strectching, respectively [12].

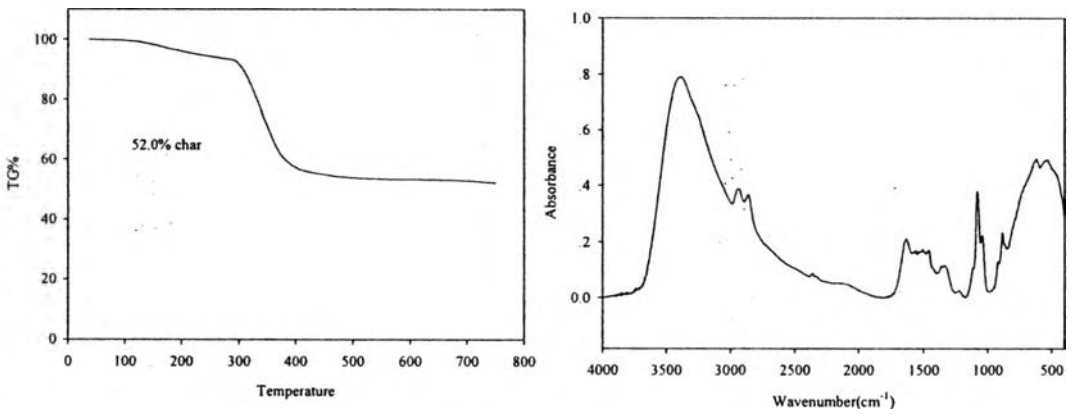

Figure 4.5 (a) TGA and (b) FTIR results of titanium glycolate precursor.

4.4.2 Characterization of Fe-, Mo-, and, Ti-SBA-15

The SAXS patterns of the calcined Fe-, Mo-, and Ti-SBA-15 samples with different M/Si (M = Fe, Mo, and, Ti) ratios are shown in Figure 4.6. They all show two well-resolved peaks which are indexed as {10} ≡ {11} and {30} ≡ {33} reflections, associated with *p6mm* hexagonal symmetry [9], indicating that the

materials have highly ordered mesoporous structure and have the same manner as pure SBA-15 [9]. When the ratios of the metal increased, the SAXS patterns of all samples still maintained the order, meaning that the amount of metal atoms do not affect to the SBA-15 network. This result probably comes from our mild synthesis conditions and extraordinary precursors having highly pure and moisture-stable properties without disturbing the order of the materials [9].

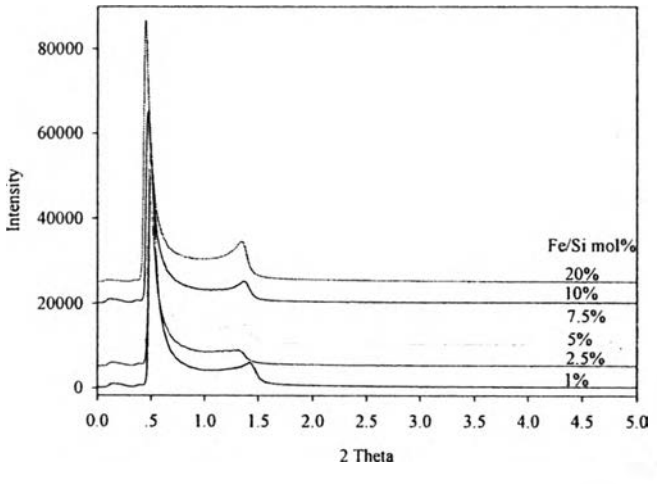

(a)

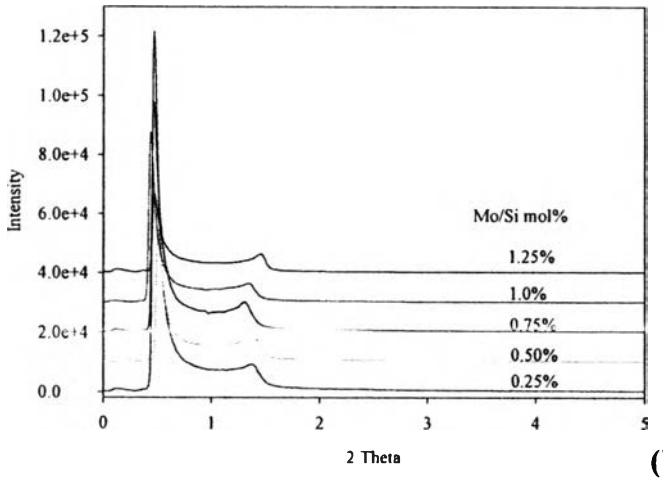

(b)

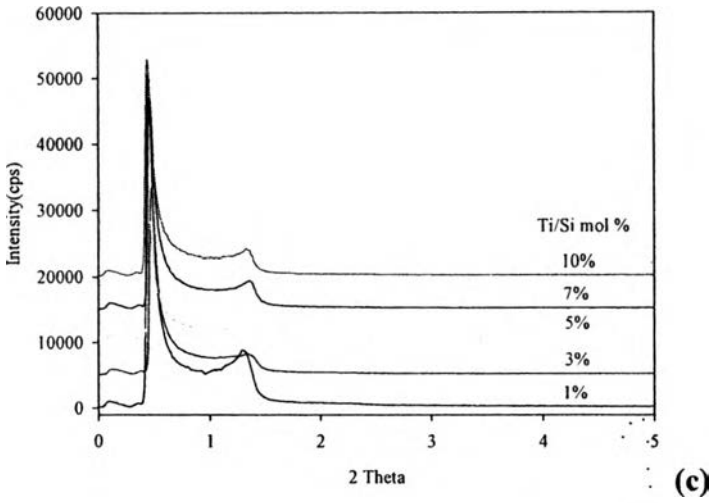

Figure 4.6 SAXS patterns of (a) Fe-SBA-15, (b) Mo-SBA-15, and (c) Ti-SBA-15 samples with various M/Si ratios.

To obtain additional information of the pore structure, the TEM images of the M-SBA-15, having the nearly highest metal ratio without disturbing the SBA-15 network (10 mol% of Fe, 1 mol% of Mo, and, 7 mol% of Ti), are illustrated in Figure 4.7. The well-ordered hexagonal array of mesopore with one-dimensional channels is clearly visible [1].

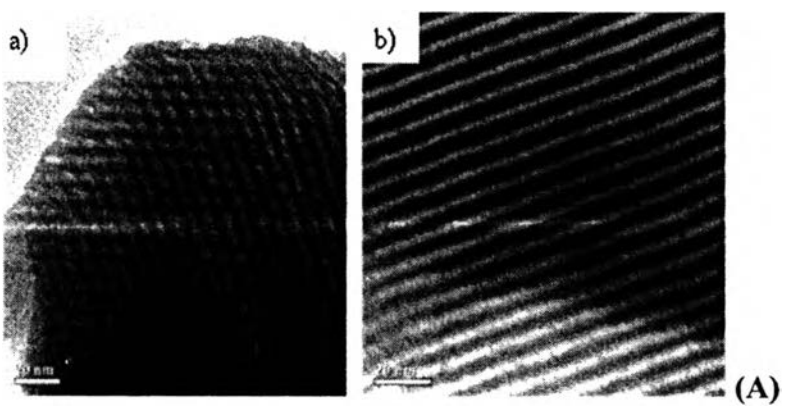

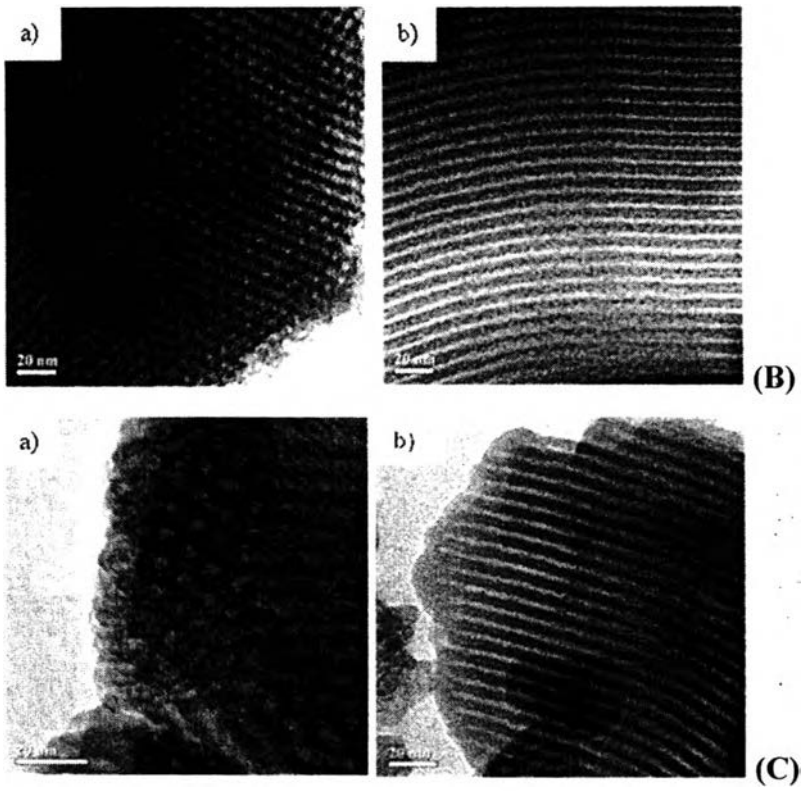

Figure 4.7 TEM images of (A) 10 mol% Fe-SBA-15, (B) 1 mol% Mo-SBA-15, and (C) 7 mol% Ti-SBA-15, in which a) in the direction perpendicular to the pore axis and b) in the direction parallel to the pore axis.

N_2 adsorption/desorption isotherms and pore size distribution patterns give further detail of the pore structures of all M-SBA-15 samples (Figures 4.8–4.10). All samples exhibit type IV isotherm, according to IUPAC classification, with H1 type hysteresis loop which is the characteristic of large-pore mesoporous solid with narrow pore size distribution [1]. The well-defined step at relatively high pressure of 0.5–0.7 corresponded to capillary condensation of N_2, indicating that these materials have the uniformity of the pores. They all showed a large pore diameter (> 5 nm) and high surface area (upto 700 m^2/g). BET surface area, pore volume, and BJH pore size of the all materials are summarized in the Table 4.1. For Fe-SBA-15 and Mo-SBA-15, the BET surface area and the pore volume did not depend on the amount of the incorporated metals, but the pore size tended to increase

with increasing the metal loadings. Similarly, for Ti-SBA-15 samples, the BET surface area and pore size slightly decreased with increasing of Ti/Si ratios.

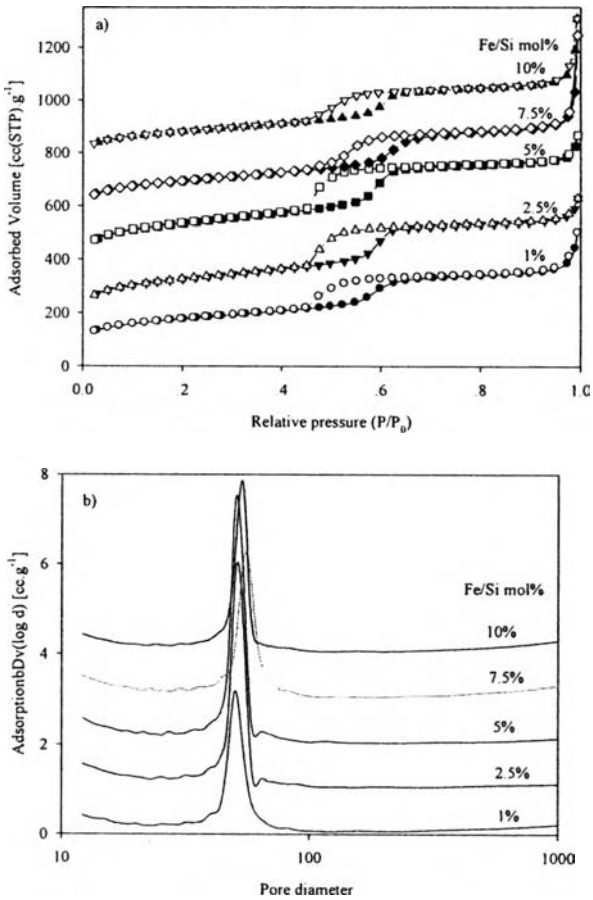

Figure 4.8 a) N_2 adsorption/desorption isotherms and b) pore size distribution patterns of Fe-SBA-15 samples with various amounts of Fe.

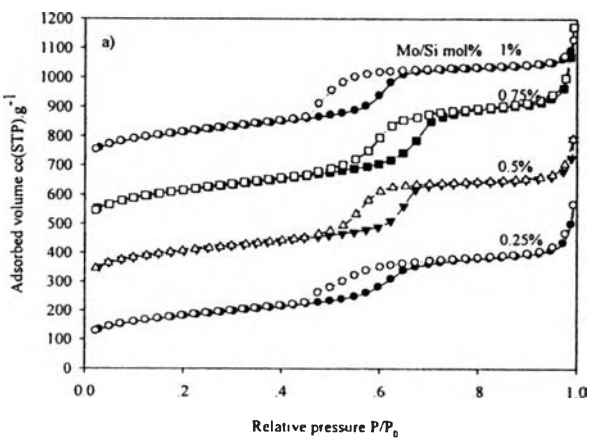

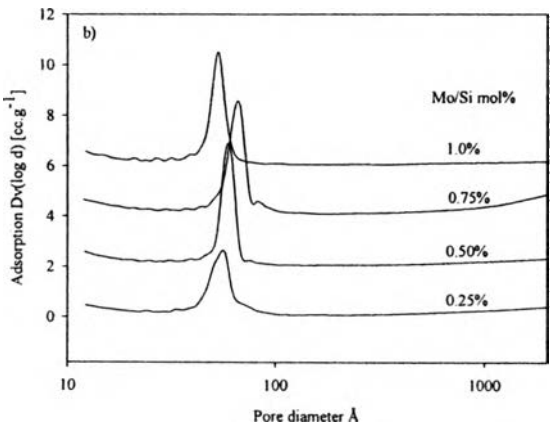

Figure 4.9 a) N_2 adsorption/desorption isotherms and b) pore size distribution patterns of Mo-SBA-15 samples with various amounts of Mo.

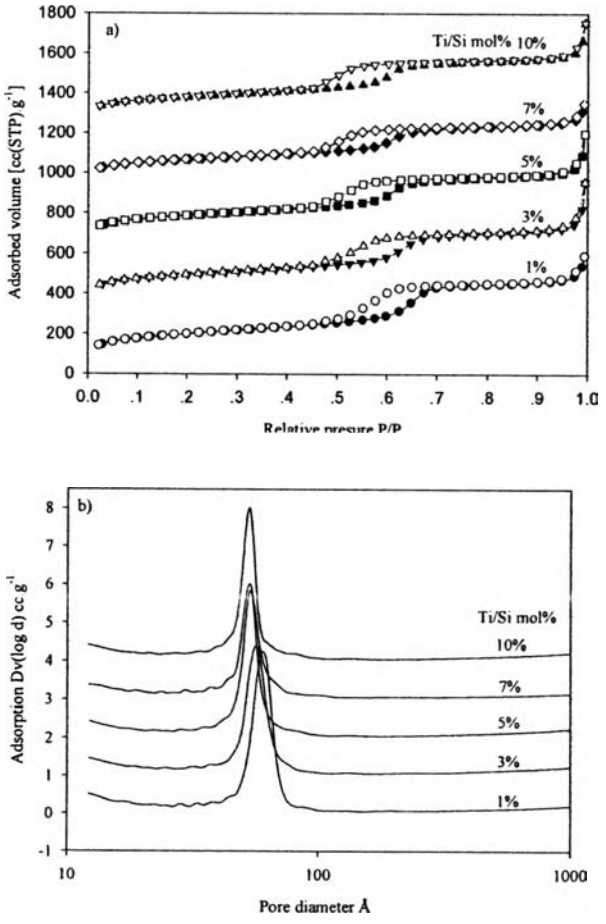

Figure 4.10 a) N_2 adsorption/desorption isotherms and b) pore size distribution patterns of Ti-SBA-15 samples with various amounts of Ti.

Table 4.1 The BET analysis of Fe-SBA-15, Mo-SBA-15 and Ti-SBA-15 synthesized with various amounts of Fe, Mo, and, Ti loadings

Sample	BET surface area (m^2/g)	Pore volume (cc/g)	Average pore size (nm)
1.0 mol% Fe-SBA-15	588	0.69	5.02
2.5 mol% Fe-SBA-15	751	0.74	5.03
5.0 mol% Fe-SBA-15	710	0.93	5.04
7.5 mol% Fe-SBA-15	715	0.73	5.37
10 mol% Fe-SBA-15	601	0.75	5.34
0.25 mol% Mo-SBA-15	607	0.77	5.38
0.50 mol% Mo-SBA-15	687	0.81	5.77
0.75 mol% Mo-SBA-15	729	1.04	6.76
1.0 mol% Mo-SBA-15	708	0.76	5.38
1.0mol% Ti-SBA-15	670	0.83	5.79
3.0mol% Ti-SBA-15	643	0.81	5.77
5.0mol% Ti-SBA-15	618	0.76	5.40
7.0mol% Ti-SBA-15	592	0.67	5.39
10.0mol% Ti-SBA-15	597	0.71	5.37

DR-UV spectra of the calcined Fe-SBA-15 samples, as shown in Figure 4.11a, showed strong absorption band at about 210–250 nm, associated with ligand-to-metal charge transfer of isolated 4-coordinated Fe^{3+}. No significant absorption at the wavelength longer than 320 nm was observed, indicating that the calcined Fe-SBA-15 samples are free from iron oligomer and an aggregated Fe_2O_3 cluster [6]. However, absorption band centered about 320 nm was observed when the Fe/Si molar ratio was up to 0.15, meaning that the iron extra-framework started to

form in the sample. Therefore, the upper limit of the iron capable to incorporate into the SBA-15 framework should be lower than 0.15 Fe/Si molar ratio.

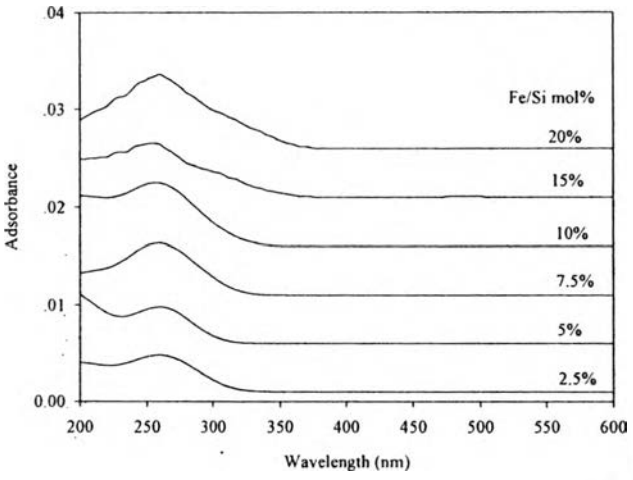

(a)

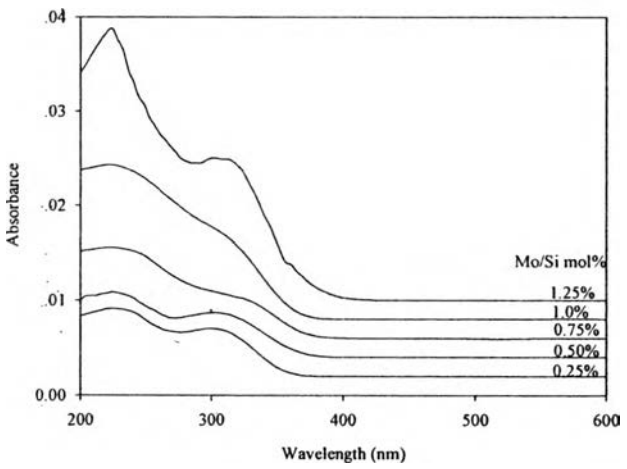

(b)

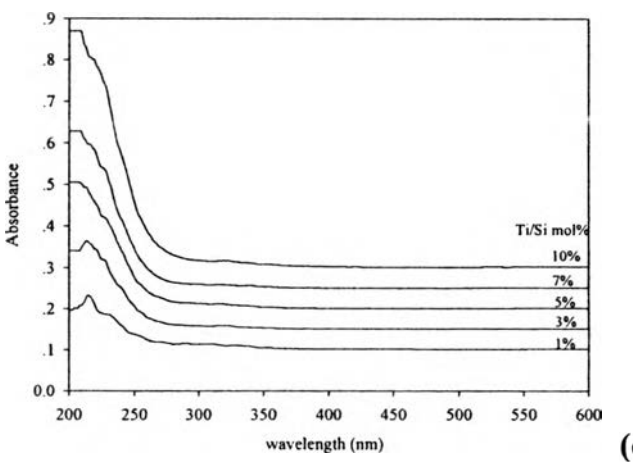

(c)

Figure 4.11 DRUV spectra of the calcined (a) Fe-SBA-15, (b) Mo-SBA-15, and (c) Ti-SBA-15 samples containing various amounts of metal.

From Figure 4.11b, DRUV spectra of Mo-SBA-15 materials have two strong adsorption bands at about 220–250 nm and 290 nm. The former is usually attributed to the presence of isolated tetrahedral Mo^{6+} species of mono- and dioxo-molybdenum species, indicating that the MoO^{4-} species incorporated into the framework via Mo-O-Si bridge, and the latter refers to the electronic transitions caused by Mo-O-Mo bond from molybdenum oligomer species [8]. The tail of peaks at about 340–400 nm of the 1.25% Mo-SBA-15 sample suggested that there was extra-framework MoO_3 formed in the material [13].

DR-UV spectra of Ti-SBA-15 samples (Figure 4.11c) showed the maximum peak at about 220 nm which is typical of ligand-to-metal charge transfer transition in TiO_4 or $HOTiO_3$, meaning that titanium atoms were incorporated into the SBA-15 framework without any extra-framework. When the Ti/Si molar ratio was up to 0.10 a peak centered at about 330 nm, indicating the extra-framework of TiO_2 was observed [7]. It means that the amount of titanium capable to incorporate into the SBA-15 framework should be lower than 0.10 Ti/Si molar ratio.

4.4.3 Activity Study of Synthesized Ti-SBA-15

Catalytic study of Ti-SBA-15 was assessed on the oxidation of styrene monomer using 30% H_2O_2 as an oxidant and acetronitrile as solvent. Figure 4.12, showing the effect of the reaction time at 80 °C reaction temperature toward the catalytic behavior, depicted the influence of the reaction time on the catalytic behavior of the 7% Ti-SBA-15. As response parameters, the conversion of styrene and the selectivity toward the products (benzaldehyde and styrene oxide) were selected. As expected, the styrene conversion increased with time, whereas the selectivity toward styrene oxide decreased. This could be attributed to the secondary oxidation of styrene oxide [4]. The reaction is fast at the beginning due to the total amount of H_2O_2 added at the beginning of the reaction [14]. The conversion of

styrene reached the maximum at 4 h and stayed rather constant after this point. Thus, the reaction time at 4 h was chosen for the next study.

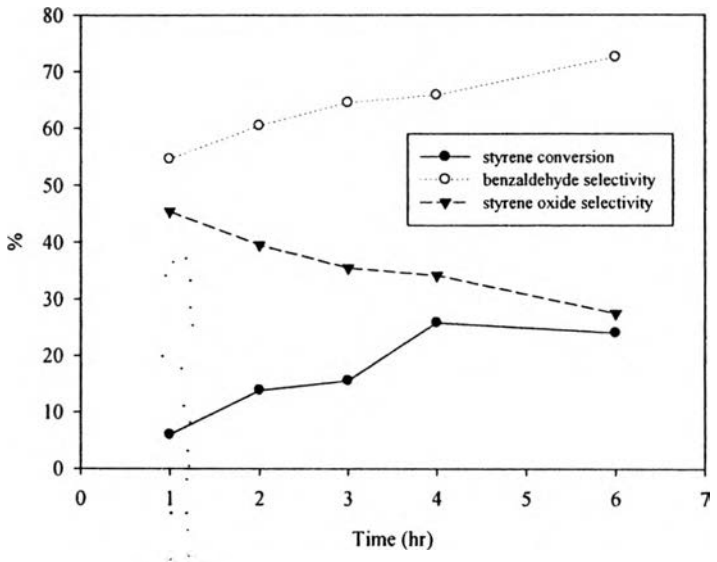

Figure 4.12 Effect of reaction time on the styrene oxidation using 0.1 g of catalyst, containing 7.0% titanium content, at 80 °C.

The conversion of styrene slightly increased with increasing the temperatures from 70 to 90 °C (Figure 4.13) which is consistent with the work of Laha *et al.* (2001). The selectivity of the catalyst toward the styrene oxide reached the highest level at 80 °C reaction temperature and decreased at higher temperature, vice versa. The selectivity of benzaldehyde also increased with increasing the reaction temperature, meaning that the higher temperature favors the further oxidation of styrene oxide [14]. Hence, the reaction temperature for the rest of the catalytic tests was set at 80 °C.

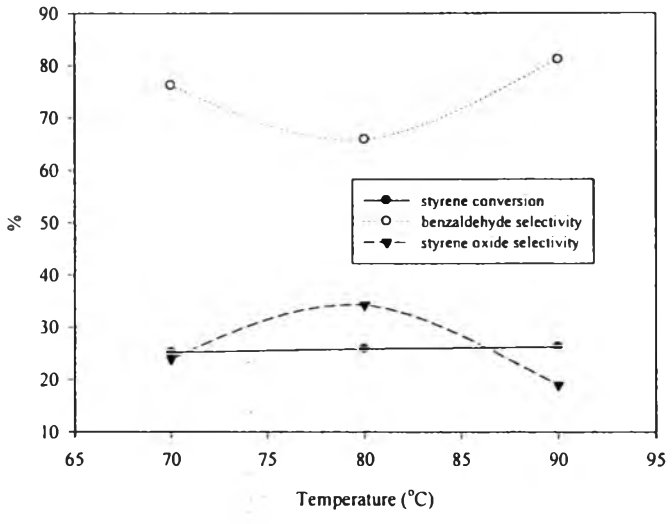

Figure 4.13 Effect of reaction temperature on the styrene oxidation using 0.1 g of catalyst, containing 7.0% titanium content, for 4 h.

The influence of the catalyst amount used is shown in Figure 4.14. The conversion of styrene increased from 11.2 % to 25.8 % with increasing the amount of catalyst from 0.05 g to 0.10 g and kept fairly constant at the higher amount of catalysts used (0.15 and 0.20 g). This result can be explained that an increase of the catalyst amount leads to an increase of Ti active site in the system, facilitating the styrene conversion [15]. The epoxidation selectivity tended to decrease with increasing the amount of catalyst higher than 0.10 g. This phenomenon may be resulted from the epoxide ring opening caused by Ti-OOH species to interact with water molecules to form the acid centers that are able to catalyze the reaction [15]. Therefore, the optimum catalyst used is 0.1 g.

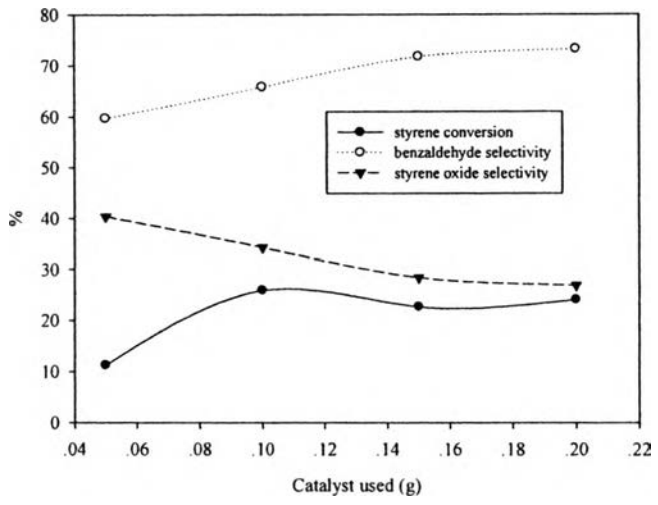

Figure 4.14 Effect of amount of catalyst, containing 7.0% titanium content, used on the styrene oxidation for 4 h at 80 °C.

The last influence factor is the titanium contents loaded into the SBA-15 network. The results are shown in Figure 4.15, giving only benzaldehyde and styrene oxide. All titanium-containing-SBA-15 samples showed considerably higher styrene conversion than pure SBA-15. The conversion of the styrene monomer was also strongly dependent of the titanium content in the catalyst because it increased from 4.0 to 25.8 % when the titanium contents increased from 0 to 7.0 %. This result is in agreement with the works of Zhang *et al.* (2002) and Ji *et al.*, (2005), indicating that the titanium species in the SBA-15 framework are the active site for the oxidation reaction [7,14]. When the titanium extra-framework presented in the SBA-15 framework (10 mol% Ti-SBA-15 sample), the conversion of styrene drastically decreased to 12.36 %. This result probably stemmed from the occupancy of the titanium extra-framework on the surface of the catalyst, meaning that the Ti^{4+} species incorporated inside the framework take responsibility to the epoxidation of styrene [4].

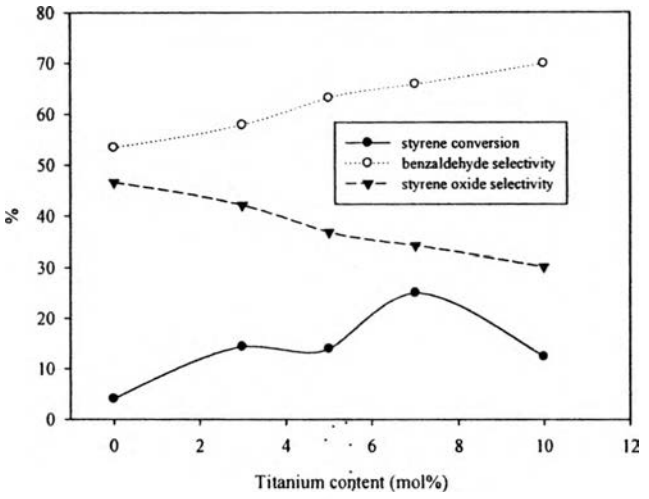

Figure 4.15 Effect of titanium content on the styrene oxidation using 0.1 g of catalyst at 80 °C for 4 h.

4.5 Conclusions

Fe-, Mo-, and Ti-SBA-15 were successfully synthesized via the novel room temperature route using silatrane precursor as a silica source and $PEO_{20}PPO_{70}PEO_{20}$ as a structure-directing agent in an acidic media at room temperature. Ferric chloride, molybdenum glycolate and titanium glycolate were used as iron, molybdenum and titanium sources, respectively. All materials still maintain well order mesostructure, high surface area (upto 700 m^2/g) and large pore size ($\geq$5 nm). The extra-framework of iron or iron oxide cluster of Fe_2O_3 was observed at Fe content upper than 10%. Different molybdenum species (mono, dioxo, and oligomeric molybdenum species) were detected on to the final Mo-SBA-15 samples with no sign of aggregated MoO_3 at the molybdenum content upto 1% Titanium species were incorporated into the silica framework upto 7% without any extra framework. Moreover, Ti-SBA-15 materials show higher activity in the oxidation reaction of styrene monomers than the pure SBA-15 due to the presence of titanium species in the SBA-15 framework. The optimum condition for styrene oxidation is at 80 °C reaction temperature for 4 h using 0.1 g of catalyst containing 7.0 % of titanium, giving only benzaldehyde and styrene oxide products.

4.6 Acknowledgements

The author is grateful for the scholarship and funding of the thesis work provided by the Petroleum and Petrochemical College; and the National Center for Petroleum, Petrochemicals, and Advanced Materials.

4.7 References

1. Zhao, D., Huo, Q., Feng, J., Chmelka, B. F., Stucky, G. D., (1998) Nonionic triblock and star diblock copolymer and oligomeric surfactant syntheses of highly ordered, hydrothermally stable, mesopotous silica structures. Journal of American chemistry society, 120(12), 6024-6036.
2. Thitsartarn, W., Gulari, E., Wongkasemjit, S., (2008) Synthesis of Fe-MCM-41 from silatrane and FeCl3 via sol-gel process and its epoxidation activity. Applied Organometallic Chemistry, 22, 97-103.
3. Wongkasemjit, S., Tamuang, S., Tanglumlert, W., Imae, T., (2009) Synthesis of Mo-SBA-1 catalyst via sol-gel process and its activity. Materials Chemistry and Physics, 117, 301-306.
4. Tanglumlert, W., Imae, T., White, T. J., Wongkasemjit, S. (2009) Styrene oxidation with H_2O_2 over Fe- and Ti-SBA-1 mesoporous silica. Catalysis Communications, 10, 1070-1073.
5. Zhang, L., Hua, Z., Dong, L., Chen, H., Shi, J., (2007) Preparation of highly ordered Fe-SBA-15 by physical-vapor-infiltration and their application to liquid phase selectivity oxidation of styrene. Journal of Molecular Catalysis A: Chemical, 268, 155-162.
6. Li, Y., Feng, Z., Lian, Y., Sun, K., Zhang, L., Jia, G., Yang, Q., Li, C., (2005) Direct synthesis of highly ordered Fe-SBA-15 mesoporous materials under weak acid conditions. Microporous and Mesoporous Materials, 84, 41-49.
7. Zhang, W., Lu, J., Han, B., Li, M., Xiu, J., Ying, P., Li, C., (2002) Direct synthesis and characterization of Titanium-substituted mesoporous molecular sieve SBA-15. Chemistry of Materials, 14, 3413-3421

8. Melero, J.A., Iglesias, J., Arsuaga, J.M., Sainz-Pardo, J., de Frutos, P., Blazquez, S., (2007) Synthesis, Characterization and catalytic activity of highly dispersed Mo-SBA-15. Applied Catalysis A: General, 331, 84-94.

9. Samran, B., White, T., Wongkasemjit, S., (2008) A novel room temperature synthesis of mesoporous SBA-15 (submitted).

10. Piboonchaisit, P.,Wongkasemjit, S., Laine, R. M. (1999) A novel Route to tris(silatranyloxy-*i*-propyl)amine directly from silica and triisopropanolamine, part 1. Science Asia, 25, 113-119.

11. Sutara, S., Gulari, E., and Wongkasemjit, S. (2004) Proceeding of the International Conference on SmartMaterial (SmartMat-'04) December 1-3, 2004, Chiang Mai, Thailand.

12. Phonthammachai, N., Chairassameewong, T., Gulari, E., Jamieson, A.M., Wongkasemjit, S. (2002) Oxide one pot synthesis of a novel titanium glycolate and its pyrolysis, Journal of metals, materials and minerals, 12, 23-28.

13. Higashimoto, S., Hu, Y., Tsumura, R., Iino, K., Matsuoka, M., Yamashita, H., Shul, Y., Che, M., Anpo, M. (2005) Synthesis, characterization and photocatalytic reactivites of Mo-MCM-41 mesoporous molecular sieves: Effect of the Mo content on local structures of Mo-Oxides, Journal of catalysis, 235, 272-278.

14. Ji, D., Zhao, R., Lv, G., Qian, G., Yan, L., Suo, J., (2005) Direct synthesis, characterization and catalytic performance of novel Ti-SBA-1 cubic mesoporous molecular sieves. Applied Catalysis A : General, 281, 39-45.

15. Laha, S.C. and Kumar, R. (2001) Selective Epoxidation of styrene to styrene oxide over TS-1 using urea-hydrogen peroxide as oxidizing agent. Journal of catalysis, 204, 64-70.